Journal of Inflammation Research

Dovepress

open access to scientific and medical research

Open Access Full Text Article

ORIGINAL RESEARCH

RETRACTED ARTICLE: Benzimidazole Derivatives as New Potential NLRP3 Inflammasome Inhibitors That Provide Neuroprotection in a Rodent Model of Neurodegeneration and Memory Impairment

Aman Ullah[1], Lina Tariq Al Kury[2], Yusuf S Althobaiti[3,4], Tahir Ali[5], Fawad ALi Shah[1]

[1]Department of Pharmacology, Faculty of Pharmaceutical Sciences, Riphah International University, Islamabad, Pakistan; [2]College of Natural and Health Sciences, Zayed University, Abu Dhabi, United Arab Emirates; [3]Department of Pharmacology and Toxicology, College of Pharmacy, Taif University, Taif, 21944, Saudi Arabia; [4]Addiction and Neuroscience Research Unit, Taif University, Taif, 21944, Saudi Arabia; [5]University of Calgary, Calgary, AB, Canada

Correspondence: Fawad ALi Shah; Yusuf S Althobaiti, Tel +923460474193; +966544583[illegible], Email fawad.shah@riphah.edu.pk; ys.althobaiti@tu.edu.sa

Objective: The study investigated the effect of newly synthesized benzimidazole derivatives against ethanol-induced neurodegeneration. According to evidence, ethanol consumption may cause a severe insult to the central nervous system (CNS), resulting in mental retardation, neuronal degeneration, and oxidative stress. Targeting neuroinflammation and oxidative stress may be a useful strategy for preventing ethanol-induced neurodegeneration.

Methodology: Firstly, the newly synthesized compounds were subjected to molecular simulation and docking in order to predict ligand binding status. Later, for in vivo observations, adult male Sprague Dawley rats were used for studying behavioral and oxidative stress markers. ELIZA kits were used to analyse tumour necrosis factor-alpha (TNF-), nuclear factor-B (NF-B), interleukin (IL-18), and pyrin domain-containing protein 3 (NLRP3) expression while Western blotting was used to measure IL-1 and Caspase-1 expression.

Results: Our findings suggested that altered levels of antioxidant enzymes were associated with elevated levels of TNF-α, NF-B, IL-1, IL-18, Caspase-1, and NLRP3 in the ethanol-treated group. Furthermore, ethanol also caused memory impairment in rats, as measured by behavioural tests. Pretreatment using selected benzimidazole significantly increased the combat of the brain against ethanol-induced oxidative stress. The neuroprotective effects of benzimidazole derivatives were promoted by their free radical scavenging activity, augmentation of endogenous antioxidant proteins (GST, GSH), and amelioration of lipid peroxide (LPO) and other pro-inflammatory mediators. Molecular docking and molecular simulation studies further supported our hypothesis that the synthetic compounds Ca and Cb had an excellent binding affinity with proper bond formation with their targets (TNF-α and NLRP3).

Conclusion: It revealed that these benzimidazole derivatives can reduce ethanol-induced neuronal toxicity by regulating the expression of cytokines, antioxidant enzymes, and the inflammatory cascade.

Keywords: benzimidazole derivatives, ethanol, neuroinflammation, neurodegeneration, oxidative stress, NLRP3 inhibition

Introduction

Neurodegenerative diseases represent a more significant hazard to humans, more precisely to the elderly population.[1] Despite the high prevalence, limited or no disease-modifying therapy (DMT) is available to manage these disorders, thus emphasizing a considerable translational gap from drug development to in vivo experimentation and clinical trials.[2,3] Several heterocyclic moieties such as benzimidazole showed favorable biological activities due to the innate structural diversity, which offers structure modulation to a greater extent. Many benzimidazoles are available as potential clinical drugs against many diseases, for instance, omeprazole and many antimicrobial agents such as albendazole and flubendazole.[4] Furthermore, many benzimidazoles are screened for their potential anti-inflammatory,[5] antiviral[6]

Received: 7 December 2021
Accepted: 16 June 2022
Published: 11 July 2022

antiproliferative, and anthelmintic properties.[7] Likely, these compounds exhibited potent free radical scavenging properties as demonstrated in several reports,[8,9] which can be attributed to neuroprotection in Parkinson's,[10] Alzheimer's,[11] and other memory impairment models.[12,13] In this context, the beneficial effects of benzimidazole against multiple neurodegenerative's targets have been recently reviewed.[14] Previously reported mechanistic studies showed that benzimidazole mediates anti-inflammatory effects by inhibiting NF-κB.[15]

We employed ethanol to generate neuroinflammation, neurodegeneration, and behavioural abnormalities as a model of memory impairment. Moreover, mounting evidence suggests that ethanol consumption may produce a severe insult to the central nervous system (CNS), resulting in negative consequences in the brain and is a main cause of birth abnormalities, mental retardation, and neurodevelopmental problems. Several mechanisms for ethanol-induced neuronal degeneration have been researched and postulated; the most well-known process is the formation of enhanced reactive oxygen species (ROS), which increases oxidative stress and, as a result, leads to neuronal degeneration.[16] Neuroinflammation is the next, which is induced by oxidative stress, also affects neuronal function.[13,17] The influx of inflammatory mediators and cytokines leads macrophages to penetrate the brain, exacerbating the underlying pathophysiology.[18] The NLRP3 inflammasome plays a significant role in innate immunity and is, therefore, the most investigated inflammasome.[19] Mitochondrial dysfunction has been suggested to accelerate neurodegeneration due to elevated reactive oxygen species (ROS) production and NLRP3 inflammasome activation in neurodegenerative and other inflammatory diseases.[20] Activation of NLRP3 inflammasome involves a two-step process. First, the activation of the nuclear factor-kappa B (NF-κB) pathway is required to upregulate the expression of NLRP3, pro-interleukin-1β (pro-IL-1β), and caspase 1, which is accomplished by stimulating toll-like receptors (TLRs).[16,21] After priming, the NLRP3 complex can be activated by several stimuli, including extracellular ATP, ionic flux, lysosomal rupture, and reactive oxygen species (ROS).[17,18]

Based on these aforementioned studies, the present study continues and further validates our previous research work by using synthetic benzimidazole as potential neuroprotective agents.[12] In this research work, we synthesized new analogs of benzimidazole, performed its structural analysis, and further evaluated its effect on oxidative stress and neuroinflammation. The results will additionally add and evidence our approach about the potential of benzimidazole for the treatment of memory impairment such as Alzheimer's disease.

Materials and Methods

Chemicals and Reagents

Daejung (South Korea) and AlfaAesar (Germany) provided all initial supplies. The melting points of the final compounds were recorded using a digital Gallenkamp (Sanyo) apparatus. The Bruker AM-300 was used to review the proton NMR (1H-NMR) and carbon-13 (13C-NMR) spectra in DMSO d6 at 300 MHz and 75 MHz, respectively, with TMS as an internal baseline. The Fourier-transform infrared spectroscopy (FTIR) spectra were recorded using an Alpha Bruker FTIR spectrophotometer (ATR eco ZnSe, Vmax in cm1). Thin-layer chromatography was used to track all reactions (TLC). Ethanol was obtained from Sigma-Aldrich Co. LLC, USA, and donepezil and dimethyl sulfoxide (DMSO) were obtained from the local pharmaceutical industry by ensuring a high analytical grade (99% HPLC-Getz Pharma). 3,3-Diaminobenzidine peroxidase (DAB), and avidin–biotin complex (ABC) were purchased from Santa Cruz Biotechnology (USA). 1-Chloro-2,4-dinitrobenzene (CDNB), hydrogen peroxide (H2O2), trichloroacetic acid (TCA), formalin, thiobarbituric acid (TBA), N-(1-naphthyl), ethylenediamine dihydrochloride, 5,5'-dithio-bis-(2-nitrobenzoic acid; DTNB), and glutathione (GSH) were procured from Sigma-Aldrich (St. Louis, MO, USA). Primary antibodies, such as mouse anti-p-NF-κB (sc-271908) and mouse anti-TNF-α (sc-52B83), and mouse anti-COX2 (SC-514489), were purchased from Santa Cruz Biotechnology (Santa Cruz, CA, USA). A secondary antibody was procured from Abcam, UK. Elisa kits for p-NF-κB (Cat # SUB28069) were procured from Shanghai Yuchun Biotechnology, China, while IL-18 ELISA kit (Cat# E-ELR0567) and TNF-A (Cat# E-EL-R0019) were purchased from Elabscience China. Rat NLRP3 Elisa kit (ab277086) was procured from Abcam, UK, while COX-2 kit (Cat # 30205Ra) was purchased from Nanjing Pars Biochem CO., LTD.

Synthesis of Benzimidazole Derivatives (Ca and Cb)

The new benzimidazole derivatives were synthesized following a three-step reaction, as shown in Figure 1 In the first step, the benzimidazole moiety was generated by the reaction of phenylenediamine with different aldehydes in the presence of sodium metabisulfite.[22] In the second step, acetanilide was added to chlorosulfonic acid and stirred at room temperature to generate 4-acetamidobenzene-1-sulfonyl chloride.[23] Finally, the newly synthesized benzimidazoles (0.01 mmol) were treated with 4-acetamidobenzene-1-sulfonyl chloride in the presence of sodium hydroxide to produce the final compounds.[24]

Docking Study

Proteins were downloaded from the PDB database. Compounds were first drawn by Chem Draw and then converted to PDB format and minimized by using PyMOL. Proteins were cleaned by PyMOL and minimized by Swiss PDB Viewer before docking. Proteins and compounds were prepared by using MGLTools. Water droplets were removed, and polar hydrogen atoms were added to all targets. Docking was performed by using AutoDock Vina[25] Grid dimensions for all marks are shown in Table 1.

Molecular Dynamic (MD) Simulation Analysis

Desmond, a package of Schrödinger LLC, was used to perform MD simulations for 50 ns. Docking studies were performed to determine the initial stages of protein and ligand complexes required for MD simulations. These molecular docking studies provide an initial prediction of the binding status of a ligand under static conditions. Simulations were conducted to predict the status of ligand binding. Protein Preparation Wizard or Maestro was used to preprocess the protein–ligand complexes, including the optimization and minimization of complexes. The system builder tool was used for the preparation of all the systems. The solvent model with an orthorhombic box was selected as a TIP3P transferable

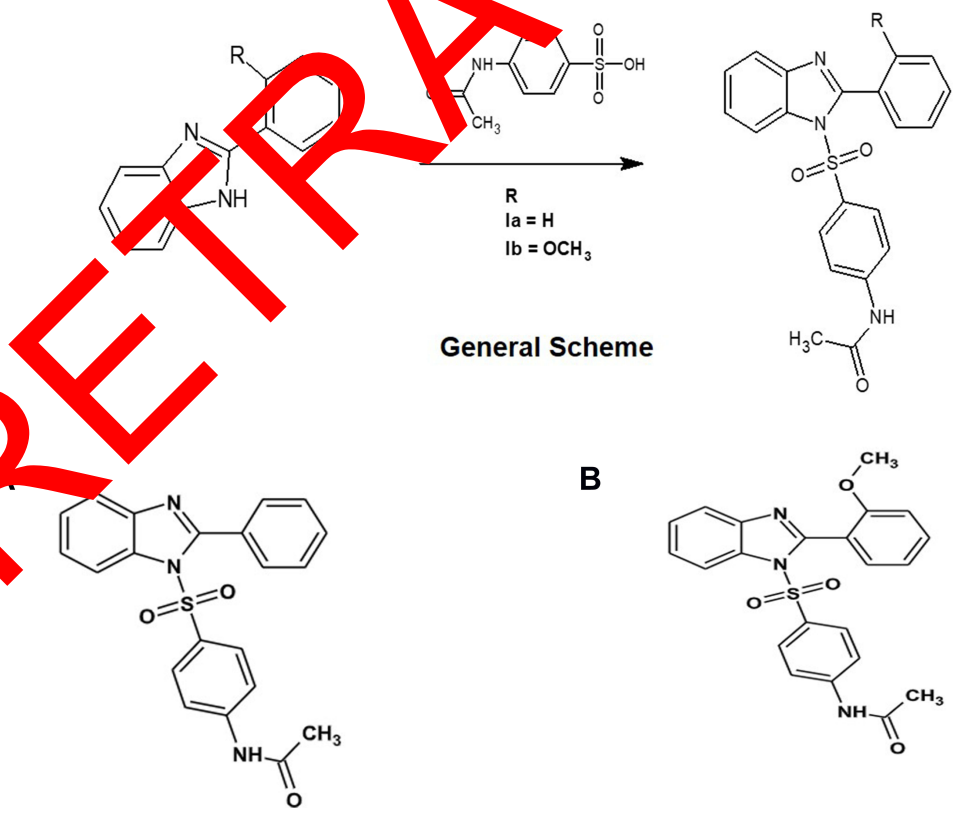

Figure 1 General scheme for the synthesis of new benzimidazole acetamide derivatives. (**A**) N-[4-(2-phenyl-1H-benzimidazole-1-sulfonyl) phenyl] acetamide (Ca) (**B**) and N-{4-[2-(2-methoxyphenyl)-1H-benzimidazole-1 sulfonyl] phenyl} acetamide (Cb).

Table 1 Grid Formation for Molecular Docking

Protein	Center_x	Center_y	Center_z	Size_x	Size_y	Size_z
5F1A	35.6756	24.9639	217.8091	76.4994210672	76.4190421867	99.0218721008
7JRA	−13.6879	71.6059	27.0007	71.6928297997	67.4812873459	71.3257006216
6NPY	105.631	104.4466	104.6186	105.028896103	78.0204025269	88.8880636597
3F62	9.9729	6.879	12.9244	48.7415888596	53.7797821236	59.9433585453

intermolecular interaction potential of 3 points. For the simulation, an OPLS_2005 force field was used. Counter ions were added to neutralize the models. And, 0.15 M salt solution of NaCl was added to mimic the physiological conditions. An NPT ensemble with a temperature of 300 K and pressure of 1 atm was selected to perform the complete simulation. The models were relaxed before the simulation studies. The stability of the simulations was evaluated by calculating the RMSD of both the protein and the ligand, and the trajectories were saved every 100 ps for analysis. Desmond trajectories were analyzed. RMSD, RMSF, and protein–ligand were calculated from the MD trajectory analysis.[26]

Animals and Drug Treatments

Adult male Sprague Dawley rats weighing 200–300 g and aged 10–12 weeks were obtained from the animal house of the Riphah Institute of Pharmaceutical Sciences. All experimental protocols were approved by the Research and Ethical Committee (REC) of the Riphah Institute of Pharmaceutical Sciences (RIPS), Riphah International University, Pakistan, and by following guidelines of the Institute of Laboratory Animal Resources, Commission on Life Sciences University, National Research Council (1996). The rats were divided into five groups, each containing n=10/group. Group I: saline group (normal saline was administered to this group for 11 days at 10 mL/kg intraperitoneally), Group II: disease group (ethanol was administered for 11 days at 2 g/kg intraperitoneally), Group III: treatment group (10 mg/kg of compound Ca was administered, followed by ethanol injection for 11 days), Group IV: treatment group (10 mg/kg of compound 6b was administered, followed by ethanol injection for 11 days), Group V: standard group (donepezil at 3mg/kg was administered, followed by ethanol injection for 11 days). The ethanol and synthetic compounds' dose were selected based on previously reported literature.[12,27] The cortex and hippocampus from the brain tissues were collected and either stored at −50°C or preserved in 4% paraformaldehyde. Histological study of tissue was performed by implanting the tissue in paraffin and sectioned into thin coronal sections (4 µm) using a rotary microtome as shown in Figure 2.

Behavioral Tests

Morris Water Maze (MWM) Test

MWM test was performed as described previously.[44] Briefly, four hypothetical quadrants were made in the cylindrical pool such as the target quadrant, left, right, and opposite quadrants. The hidden platform was positioned 1 cm beneath the water surface in the target quadrant. Training sessions were conducted for 3 days to determine the escape latency. The training sessions were carried out two times a day with a lag period of 25 min between each trial. During the probe test, the platform was removed and each animal was dropped opposite to the target quadrant. Time spent in the target quadrant was considered as a measure of the extent of memory function and impairment.

Y-Maze Test

The Y-maze apparatus consisted of a black painted wooden piece about 50-cm tall, 20-cm thick, 10-cm wide at the bottom, and 10-cm wide at the top. Each individual rat was placed in the center of the maze and allowed to move freely (up to 8 min). The entry of rats into the alternate arm was considered to be a spontaneous alternation, while the entry of rats into the adjacent arm set was denoted as a total number of arm entries. The percentage (%) of alternation behavior

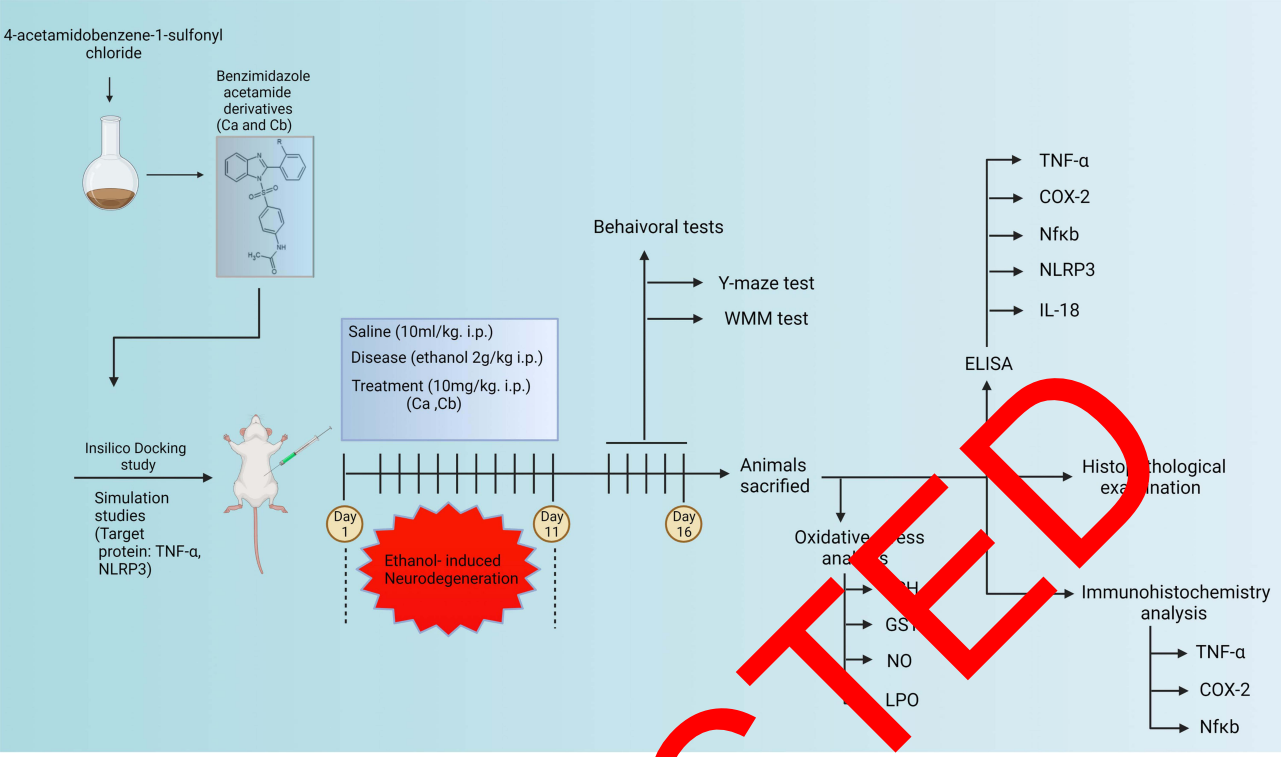

Figure 2 Experimental design.

was calculated as the number of successful entries into three different arms/total number of arm entries – 2×100. A greater percentage of alternation behavior showed enhanced spatial working memory and vice versa.[28]

Oxidative Enzyme Analysis

Glutathione (GSH) and Glutathione S-Transferase (GST) Assay

GSH level was determined as previously mentioned protocol. We mixed 0.2 mL of the tissue supernatant with 2 mL of DTNB mixture, followed by the addition of 0.2 M phosphate buffer to yield a final volume of 3 mL. The absorbance was measured after 10 min using a spectrophotometer at 412 nm, where phosphate buffer and DTNB solution were used as a blank and control respectively. The real absorbance value was obtained by subtracting the absorbance of the control from that of the tissue lysate. The final GSH activity was expressed in units of µmol/mg of protein.[27]

To calculate GST activity, we freshly prepared 1 mM CDNB and 5 mM GSH solutions in 0.1 M phosphate buffer. Three replicates of the 1 mL reaction mixture were kept in glass vials, followed by the addition of 60 µL of tissue homogenate to each of these mixtures. The blank contained water rather than tissue lysate. Next, 210 µL aliquots from the reaction mixture were pipetted out in a microtiter plate; further, absorbance was measured at 340 nm for 5 min at 23 °C using an ELISA plate reader (BioTek ELx808, Winooski, VT, USA). GST activity was expressed in units of µmol of CDNB conjugate/min/mg of protein.

Lipid Peroxide (LPO) Assay

Another major oxidative stress marker is lipid peroxide (LPO), which is measured using a colorimetric technique (thiobarbituric acid reactive substances).[29] A mixture of 200 µL of supernatant, 200 µL of 100 mM ascorbic acid, 580 µL of 0.1 M PBS (pH 7.4), and 20 µL of ferric chloride was formulated. The mixture was then maintained for 1 hour at 37 °C in a water bath. One thousand liters of 0.66% thiobarbituric acid (TBA) and 1000 L of 10% trichloroacetic acid (TCA) were added to the reaction mixture to stop the process. These sample tubes were then incubated in a water bath for another 20 minutes, then soaked in ice-cold water for a time before being centrifuged at 3000g for 10 minutes. Finally, the concentration of TBARS was

determined by measuring the absorbance of the resultant mixture at 535 nm using an adequate blank. (nM/min)/mg protein was used to compute the TBARS concentration.

Determination of Nitric Oxide (NO)

The Griess reagent reaction technique, with minor modifications, was used to quantify nitric oxide (NO) in tissue homogenate.[30] Fifty mcroliters of normal saline, 50 µL of Griess reagent (0.2% NEDD-naphthyl ethylenediamine dihydrochloride, 2% sulfanilamide in 5% phosphoric acid), and 50 µL of previously homogenized and diluted supernatant layer of brain tissue lysate were combined in a test mixture. The resultant mixture was incubated for 30 minutes at 37 °C. The absorbance of this solution at 540 nm was measured using a microplate reader. A standard sodium nitrite solution was also used to calibrate the absorbance coefficient.

Enzyme-Linked Immunoassay (ELISA)

The NF-κB, TNF-α, COX-2, NLRP3, and IL-18 ELISAs were performed according to the manufacturer's instructions. After homogenizing brain tissue (50 mg), the supernatant was extracted after centrifugation (4000 rpm for 30 min). The BCA method was used to determine the total protein concentration in each group. Using a 96-well plate, protein samples were treated with antibodies contained in the package, absorbance values were measured with a microplate reader, and concentrations in picograms per liter (pg/mL) were converted to total protein content in picograms per milligram (pg/mg total protein). All procedures were repeated three times.[31]

Morphological Analysis

Following behavioral studies, animals were euthanized to collect brain samples and were fixed in 4% paraformaldehyde for morphological analysis. The tissue was first sliced into 3–4 µm coronal sections and then embedded into paraffin blocks and cut into thin 4µm sections by a microtome, and the following techniques were applied.

Hematoxylin and Eosin (H&E) Staining

Starting from dewaxing/deparaffinization and then rehydration step using a gradient alcohol series, which was ended by rinsing slides in distilled water. Slides were then stained with hematoxylin and eosin, as discussed.[32,33] Finally, slides were dehydrated, and color was fixed in xylene and observed by a light microscope (Olympus, Japan).

Immunohistochemical Analysis

Immunostaining was performed as previously discussed.[34] The tissue was first rehydrated using xylene, graded alcohol series, and distilled water, then washed three times with PBS for 5 minutes each time. The antigen recovery process was performed with Proteinase K. To suppress endogenous peroxidase activity, the tissue was washed and then treated with a 3% H_2O_2 solution for 5 minutes. To prevent areas outside of the antigenic zones, blocking serum was administered at room temperature for at least 1 hour. The slides were then incubated overnight at 4 °C with anti-mouse COX-2, anti-mouse TNF-α and anti-mouse p-NF-B antibodies (dilution 1:100, Santa Cruz Biotechnology, Dallas, TX, USA). After washing with PBS, the slides were treated with a secondary antibody for 2 hours the next day. The slides were then stained with an ABC staining kit and allowed to dry for 1 hour. Finally, the slides were stained for 5 minutes with DAB solution, rinsed with water, dipped in xylene and 100% ethanol, then coated with a mounting medium. The slides were air-dried for at least 1 day before being photographed with an Olympus microscope and analyzed with ImageJ software. The slides were examined at 10× and 40× magnifications, with five randomly overlapping sections chosen to determine the number of labeled neurons in the cortex and hippocampal regions.

Statistical Analysis

The data are presented as mean ± SEM. Data were analyzed by one-way analysis of variance (ANOVA) followed by a post hoc Bonferroni multiple comparisons using GraphPad Prism 6 software. Immunohistochemical data were analyzed using ImageJ software (ImageJ 1.30). The symbol $ indicates a significant difference relative to saline, € shows a significant difference relative to the ethanol group. The value of $P < 0.050$ considered as level of significance.

Results

Spectral Analysis of Compound Ca

Yield: 59%; m.p: 155°C; Rf=0.71 (ethyl acetate: pet ether, 1:7); Fourier-transform infrared spectroscopy (FTIR): 3455 (NH), 3100 (CH, sp2), 2870 (CH, sp3), 1660 (NH, amide), and 1560 (C=C, aromatic). Proton nuclear magnetic resonance (HNMR) (DMSO-d6, δ ppm): 2.12 (CH3, s, 3H), 7.31–7.5 (m, Ar-H, 4H), 7.55 (d, 2H, J = 7.6 Hz), 7.6 (Ar-H, d, 2H, J = 7.0 Hz), 7.7 (Ar-H, d, 2H, J = 7.0 Hz), 7.8 (Ar-H, d, 2H, J =8.0 Hz), 7.65 (Ar-H, t, 1H, J = 8.0 Hz), and 9.10 (N-H, s, 1H).

Spectral Analysis of Compound Cb

Yield: 55%; m.p: 172°C; Rf=0.67 (ethyl acetate: pet ether, 1:7); FTIR: 3450 (NH), 3090 (CH, sp2), 2865 (CH, sp3), 1660 (NH, amide), and 1560 (C=C, aromatic). HNMR (DMSO-d6, δ ppm): 2.16 (CH3, s, 3H), 7.31–7.5 (m, Ar-H, 4H), 7.58 (d, 2H, J = 7.6 Hz), 7.64 (Ar-H, d, 2H, J = 7.0 Hz), 7.2–7.9 (Ar-H, dd, 4H, J = 7.0 Hz), 3.91 (CH3, s, 3H), and 9.10 (N-H, s, 1H).

Docking Studies and Molecular Dynamic (MD) Simulation

We performed docking studies and molecular dynamics (MD) simulations of our synthesized drugs Ca, Cb, and donepezil (DNP) used as standard here against TNF-α (PDB ID: 7JRA), COX2 (PDB: 5F1A), NLRP3 (PDB: 6NP3), and IL-18 (PDB: 3F62). The detailed binding energies and hydrogen bond formation are shown in Table 2 and 3, while 2D and 3D interactions are shown in Figure 3. Due to the significant role of TNF-α and NLRP3, we further subjected the complex to MD simulations to predict the ligand binding status. The MD simulation was performed for six complexes Ca-TNF-α, Cb-TNF-α, DNP-TNF-α, Ca-NLRP3, Cb-NLRP3, and DNP-NLRP3 for 50 ns, and results were interpreted as root mean square deviations (RMSD) (Figure 4), root mean square fluctuations (RMSF) (Figure 5), hydrogen and energy plots (Figure 6) analyses. The RMSD value reveals complex stability, and its value up to 3Å indicates stable interaction. The RMSD is estimated based on the atom selection once all protein frames are aligned on the reference frame backbone. Throughout the simulation, monitoring the protein's RMSD can provide insight into its structural conformation. The RMSD plots (Figure 4) show that both protein and ligand demonstrate stability, and different ligands remain connected in the protein's binding pocket in the simulation process. The RMSD of a ligand is shown in this plot, "lig fit prot", when the protein–ligand complex is first aligned on the reference protein backbone, and then the RMSD of the ligand heavy atoms is measured. The RMSD plot of the complexes

Table 2 Best Pose Dock Analysis, Showing Atomic Contact Energy Values (kcal/nol) Formed by the Interaction of Ca, Cb, and Donepezil Against TNF-α, COX-2, NLRP3, and IL-18

Compound	Tnf α	Cox-2	NLPR3	IL-18
Binding energies, kcal/mol				
Ca	−9.4	−9.9	−9.1	−7.9
Cb	−8.9	−8.3	−8.4	−6.7
Donepezil	−8.2	−8.8	−8.8	−6.9

Table 3 Best Pose Dock Analysis, Showing the Number of Hydrogen Bonds Formed by the Interaction of Ca, Cb, and Donepezil with TNF-α, COX-2, NLRP3, and IL-18

Compounds	Tnf α	Cox-2	NLPR3	IL-18
Number of conventional hydrogen bonds				
Ca	1	3	1	3
Cb	2	1	4	3
Donepezil	1	1	1	3

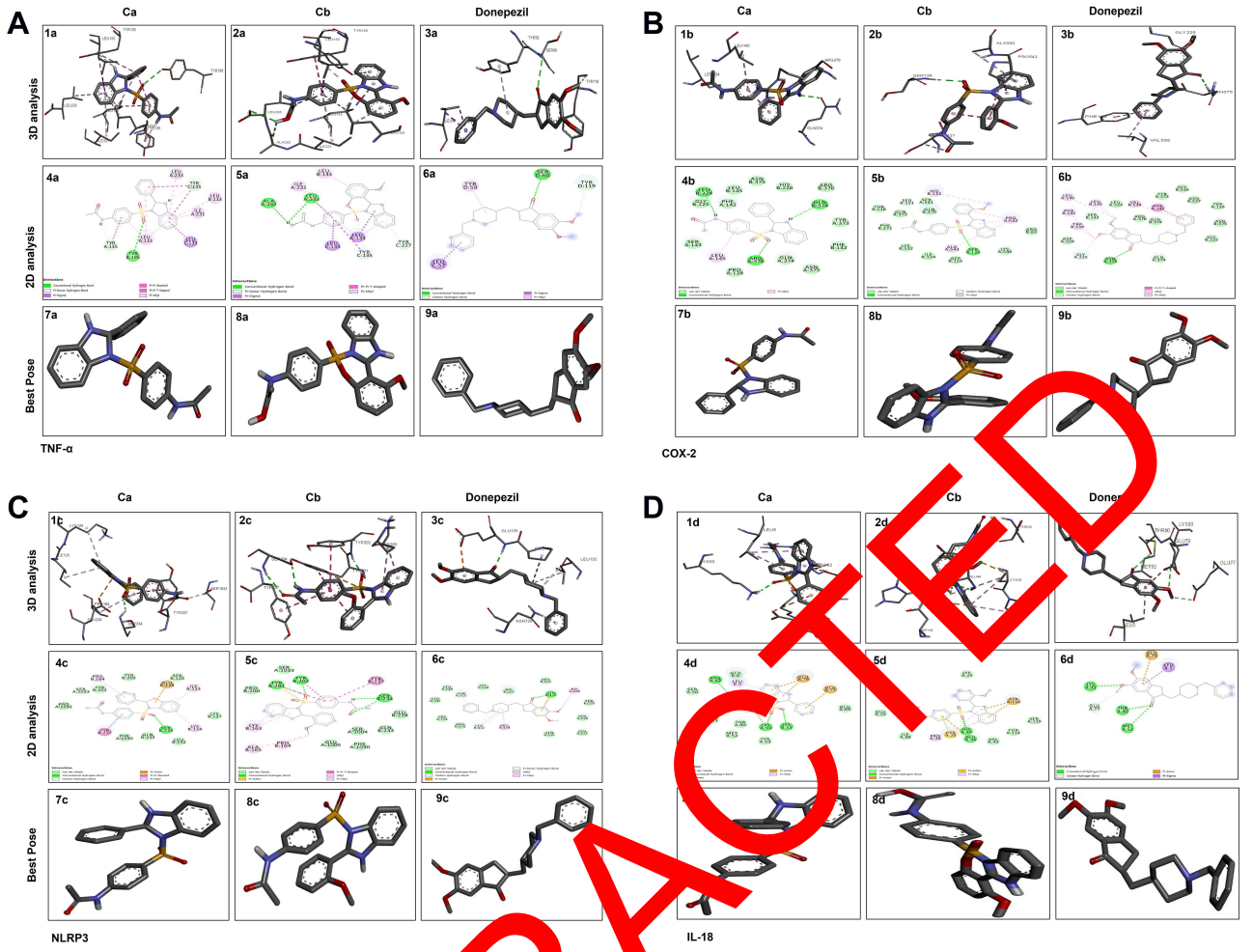

Figure 3 Docked poses of protein TNF-α (**A**), COX2 (**B**), NLRP3 (**C**), and IL-18 (**D**) with co-crystallized ligands Ca and Cb. Panel 1a, 2a, 3a, and 1b, 2b, 3b, and 1c, 2c, 3c, and 1d, 2d, 3d represent 2D interactions of Ca, Cb, and donepezil respectively with TNF-α, COX2, NLRP3, and IL-18. Panel 4a, 5a, 6a, and 4b, 5b, 6b, and 4c, 5c, 6c, and 4d, 5d, 6d represent 3D interactions of Ca, Cb, and donepezil respectively with TNF-α, COX2, NLRP3, and IL-18. Panel 7a, 8a, 9a, and 7b, 8b, 9b, and 7c, 8c, 9c, and 7d, 8d, 9d represent the best pose of the complex.

indicates that the complex Ca-TNF-α (Figure 4A), Cb-TNF-α (Figure 4C), DNP-TNF-α (Figure 4E), Ca-NLRP3 (Figure 4B), Cb-NLRP3 (Figure 4D), and DNP-NLRP3 (Figure 4F) reaches stability, respectively at 15ns, 10ns, 5ns, 5ns, 5ns, and 15ns with average RMSD values 0.4 Å, 0.6 Å, 0.5 Å, 0.8 Å, 1.5 Å, and 0.5 Å persists up to 50 ns. The RMSF value of the protein is coupled to the ligand (Figure 5). The residues with higher peaks belong to loop areas or N- and C-terminal zones, as determined by MD trajectories (Figure 6). The stability of ligand binding to the protein is shown by low RMSF values of binding site residues. Furthermore, a persistent protein–ligand association is critical for the detection of hotspots. We noticed here that TNF-α residues B-GLN125, C-SER60, C-TYR119, D-GLY121 possess the highest interaction fractions to value equal to or greater than 0.15 with Ca (Figure 6A), Cb ligand shows an interaction fractions value >0.5 for residues B-GLN125 and D-TYR151 (Figure 6B). DNP shows a value >0.8 for residue D-TYR151 (Figure 6C). On the other hand, NLRP3 produces interaction fractions of value >0.4 for all ligands, whereas two residues are involved for Ca (Figure 6D, A-GLY696, B-GLU135), while one residue for Cb (Figure 6E, A-LYS696) and one for DNP (Figure 6F, B-GLU135). These complexes also indicated a convincing interaction of amino acids using different bonds. The protein and ligand timeline interaction is represented as graphs for Ca-TNF-α complex (Figure 7A), Cb-TNF-α complex (Figure 7B), DNP-TNF-α complex (Figure 7C), Ca-NLRP3 complex (Figure 7D), Cb-NLRP3 complex (Figure 7E), DNP-NLRP3 complex (Figure 7F).

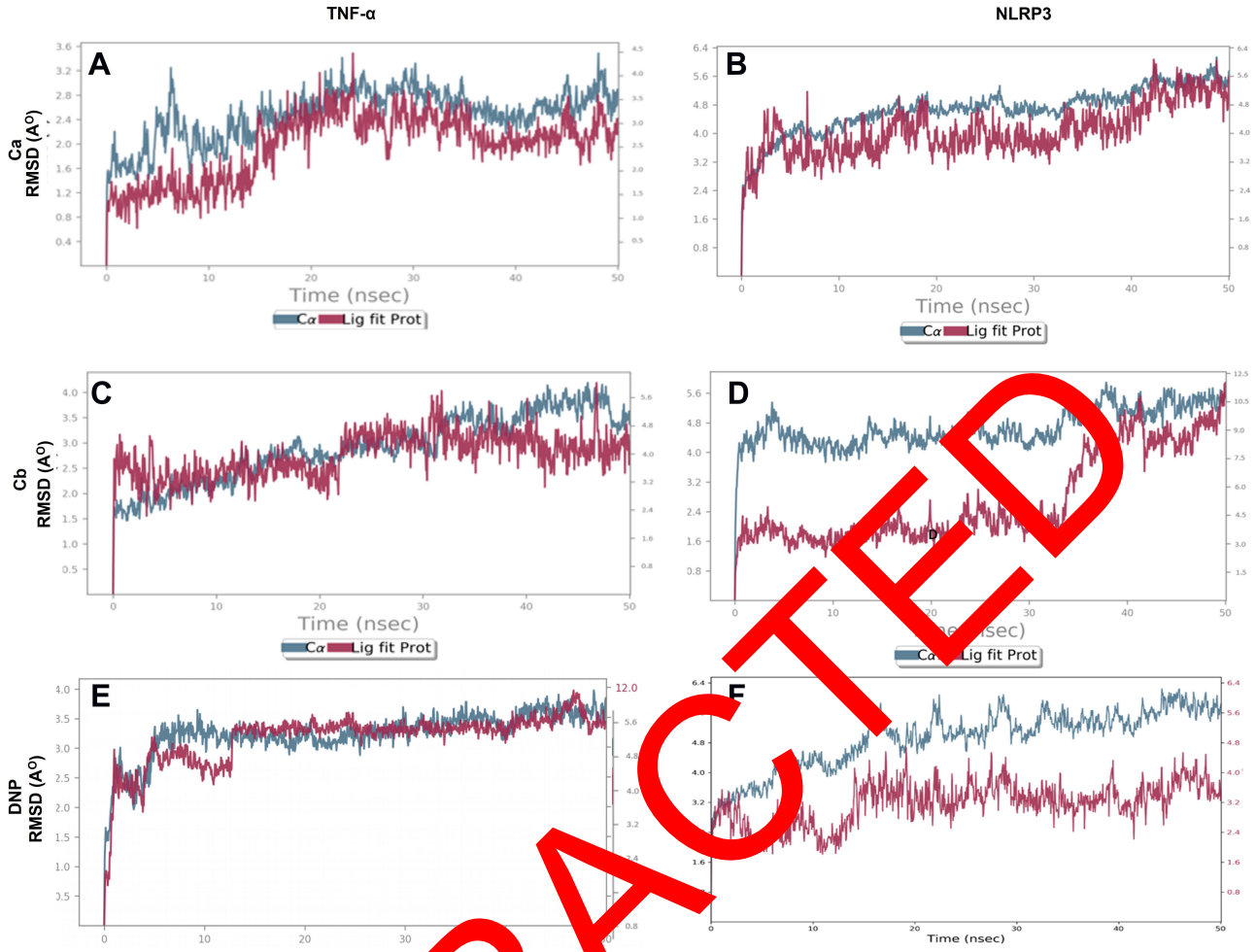

Figure 4 Representative RMSD panels of the Ca, Cb and donepezil target protein TNF-α and NLRP3 over different nanoscale times. The left and the right y-axis indicated a change in the RMSD value of the target protein and ligand respectively over different nanoscale times. (**A**) Ca-TNF-α complex, (**B**) Ca-NLRP3 complex, (**C**) Cb-TNF-α complex, (**D**) Cb-NLRP3 complex, (**E**) DNP-TNF-α complex, (**F**) DNP-NLRP3 complex.

Effect of Ca and Cb on Cognitive Impairment and Histopathology

To determine the relative role of our test compounds on cognitive deficits, we performed MWM and Y-maze tests as these tests assess hippocampus-dependent spatial learning.[28–30] In the hidden-platform test of MWM, ethanol-treated rats exhibited a longer latency time than saline-treated rats, which indicated severe memory deficits (Figure 8A, $$p < 0.01). Treatment with Ca and Cb 10 mg/kg doses significantly improved latency to reach the hidden platform (Figure 8A, €p < 0.05). To assess space memory, a probe trial was conducted 24 h after the last acquisition period. Figure 8B shows the time spent by each group of rats in different quadrants, while Figure 8C indicates percent time in the target quadrant. Increased time spent in quadrants other than the target quadrant shows impaired spatial learning, as observed in the ethanol group (Figure 8B and C, $$p<0.01). After treatment, the animals displayed significantly improved spatial memory and learning with 10mg/kg Ca and Cb (Figure 8B and C, €p < 0.05). Additionally, a Y-maze test (Figure 8D) was conducted to assess the percentage of spontaneous alternation behavior in rats. Ethanol-treated animals demonstrated a significant behavior deficit as shown by the fewer percentage of alternation in the Y-maze. On the other hand, the compounds significantly enhance the percentage of alternation compared to the ethanol-alone injected mice. Using H&E staining, we investigated morphological alterations in the cortical and hippocampus regions to further verify our concept. The saline group had spherical, well-demarcated intact cells with basophilic cytoplasm and no nuclear condensation or distortion (Figure 8E). Swollen, flattened, atrophied, and karyolitic neurons with pyknotic nuclei were observed in the

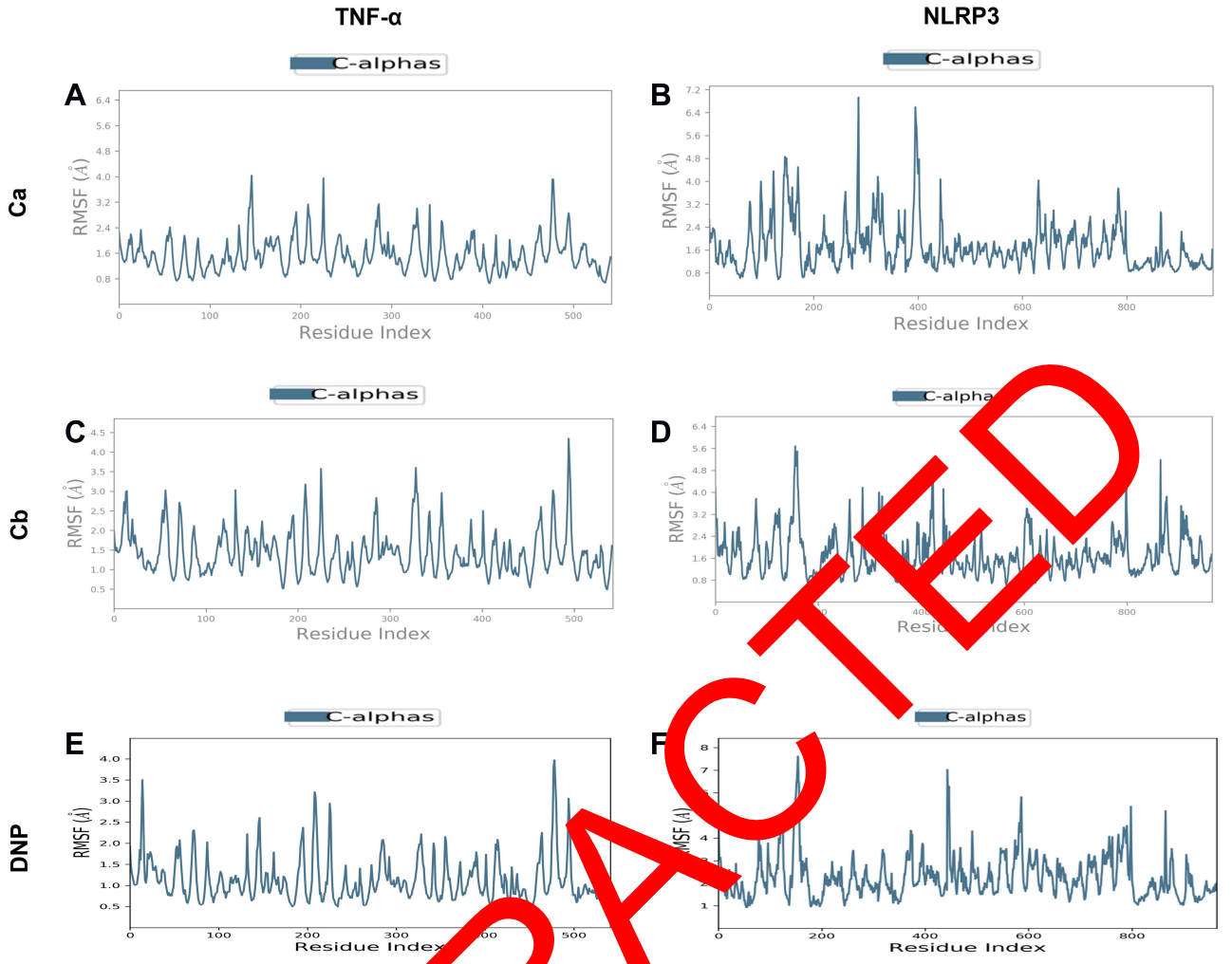

Figure 5 Representation of RMSF for the Ca, Cb, and DNP using the Desmond software package. (**A**) Ca-TNF-α complex, (**B**) Ca-NLRP3 complex, (**C**) Cb-TNF-α complex, (**D**) Cb-NLRP3 complex, (**E**) DNP-TNF-α complex, (**F**) DNP-NLRP3.

ethanol-treated group, as well as other unusual traits such as swollen, flattened, atrophied, and karyolitic neurons with pyknotic nuclei (Figure 8F). Examination of cortical and hippocampal areas validated that our newly synthesized drugs significantly ameliorate these morphological damages, as indicated by an increase in the number of intact neurons and cell count (Figure 8E, cortex: €p < 0.05 and DG: €p < 0.05).

Effect of Ca and Cb on the Endogenous Enzyme Level

We observed a significant change in the antioxidant profile between the saline and ethanol-administered rats. In the ethanol group, a considerable reduction in GST and GSH levels (Figure 9A and B, $$P<0.01) was demonstrated associated with a significant elevation in the activity of LPO (Figure 9C, $$P<0.01 and NO levels (Figure 9D, $$P<0.01). Ca and Cb reversed the effect of ethanol and normalized the antioxidant enzyme levels of GSH (€p < 0.05), GST (€p < 0.05) while reducing the elevated level of LPO and NO as shown in Figure 9C and D (€p < 0.05).

Ca and Cb Downregulated Inflammatory Cascade

Inflammatory mediators play a significant role in memory impairment. Therefore, we investigated whether Ca, Cb could influence neuroinflammation. The protein level of p-NFκB, COX-2, and TNF- α were determined in the cortex and hippocampus

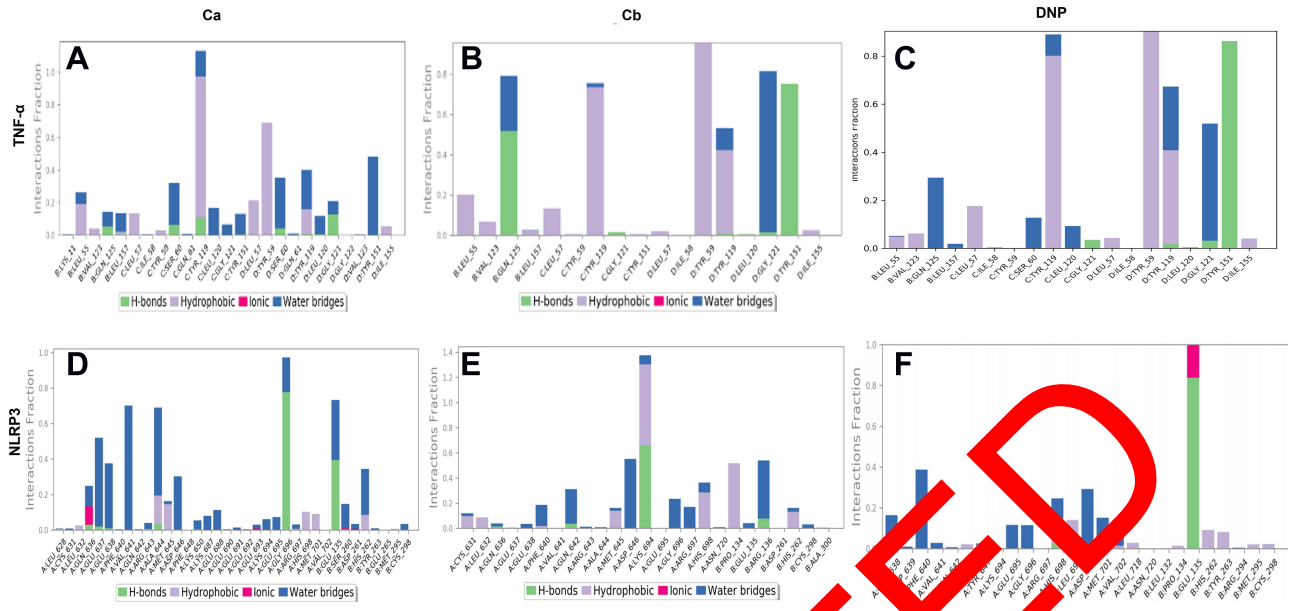

Figure 6 Interactions of drugs with receptor proteins. (**A**) Ca-TNF-α complex, (**B**) Cb-TNF-α comple[illegible] DNP-TNF-α co[illegible]) Cb-TNF-α complex, (**E**) Cb-NLRP3 complex, (**F**) DNP-NLRP3 complex.

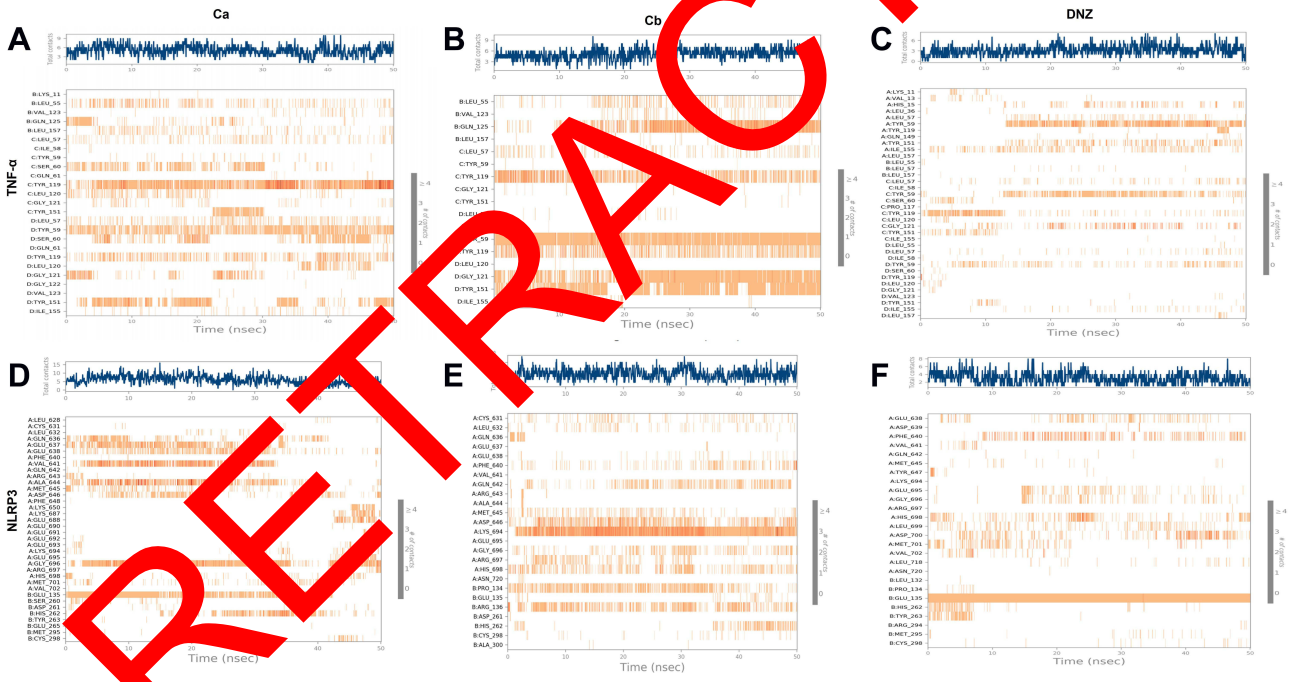

Figure 7 Timeline re[illegible]sentation of the interactions and contacts (H-bonds, hydrophobic, ionic, and water bridges) the top panel of each image shows the total number of specific contacts the protein makes with the ligand throughout the trajectory. The bottom panel of each image shows which residues interact with the ligand in each trajectory frame. (**A**) Ca-TNF-α comple,x (**B**) Cb-TNF-α complex, (**C**) DNP-TNF-α complex, (**D**) Cb-TNF-α complex, (**E**) Cb-NLRP3 complex, (**F**) DNP-NLRP3 complex.

using ELISA. The level of these proteins was significantly elevated in the ethanol group relative to the saline group (Figure 10A, C and E, $$p<0.01). Ca and Cb treatment resulted in a substantial decrease in the level of p-NFκB (Figure 10A, €p<0.05), COX-2, and TNF- α (Figure 10C and E €p<0.05). To further validate, we performed immunohistochemistry analysis of p-NFκB (Figure 10B), TNF-A (Figure 10D), and COX-2 (Figure 10F), and similar results were replicated. Furthermore, we also

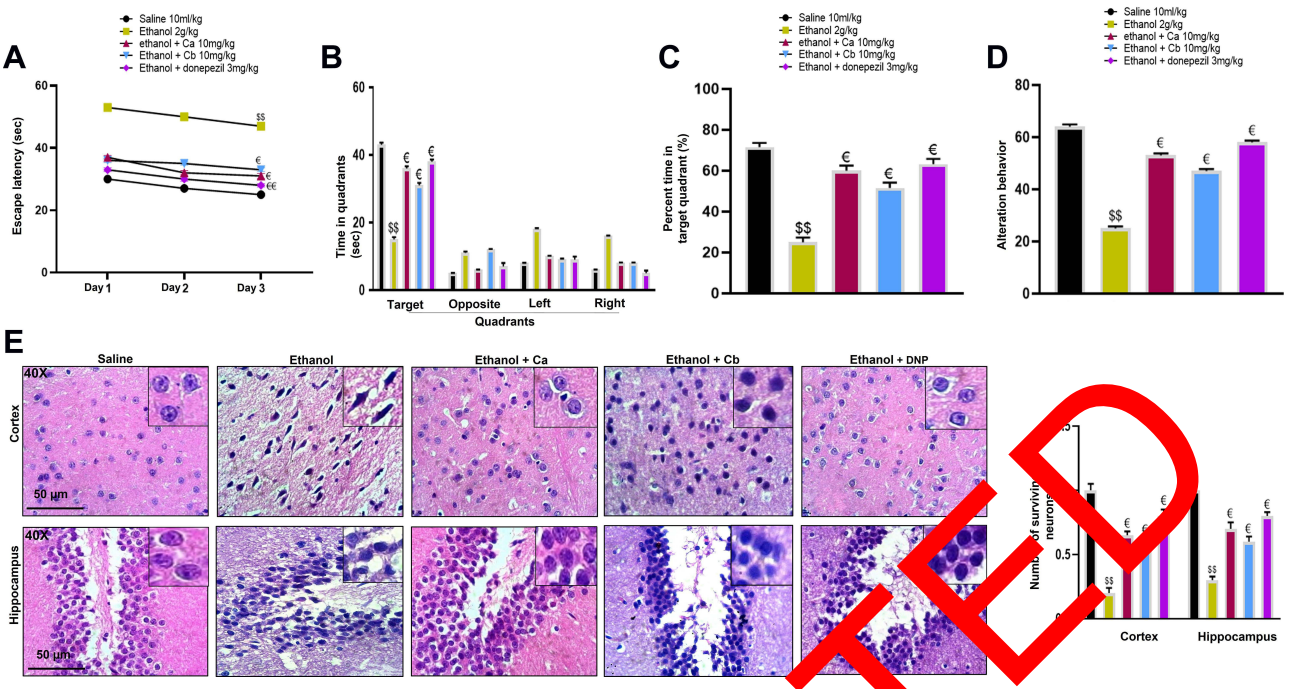

Figure 8 Effect of Ca and Cb on ethanol-induced memory impairment and neuronal survival. (**A**) The latency time of rats to the hidden platform. (**B**) Time spent by ethanol and drug-treated rats in each quadrant in the probe test on the 4th day. (**C**) The percentage time spent by animals in the target quadrant, with 10/group. (**D**) Effect of ethanol and drugs on alteration behavior. (**E**) Representative photomicrographs of the H&E-stained cortex and hippocampal tissue revealing the presence of kryolitic and atrophied nuclei in ethanol-treated animals while the Ca, Cb, and donepezil group showed only a few cells with degenerative signs (40×, scale bar 50 µm). All data were expressed as mean ± SEM (n=5/group). Data are expressed as mean ± SEM. $^{\$\$}p<0.01$ compared to the saline group, $^{€}$Shows a significant difference relative to the ethanol group denotes a significant difference compared with the saline group$^{\$\$}$.

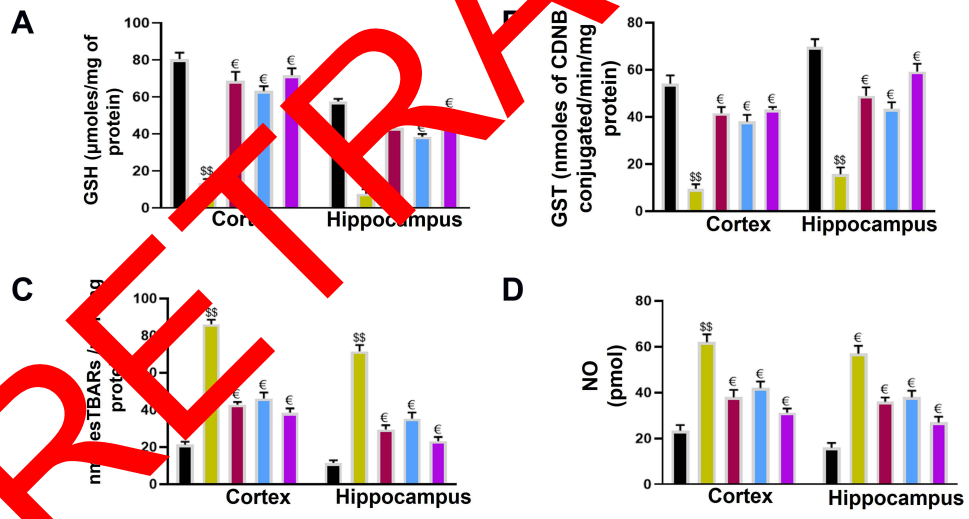

Figure 9 Effect of Ca, Cb, and donepezil on oxidative enzymes in the cortex and hippocampus. (**A**) GSH level, (**B**) GST level, (**C**) LPO level, (**D**) NOS level. Data are expressed as mean ± SEM. $^{\$\$}p<0.01$ compared to the saline group while $^{€}p<0.05$ compared to the LPS group. $^{€}$Shows a significant difference relative to the ethanol group All data were expressed as mean ± SEM (n=5/group).

investigated NLRP3 and IL-18 expression, and our results demonstrated that Ca and Cb significantly reduced the expression level of these proteins relative to the ethanol group (Figure 10G and H, €p<0.05). Western blot analysis demonstrated that the IL-1β and Caspase-1 expression level in the ethanol-treated group was significantly high compared to that in the saline-treated group

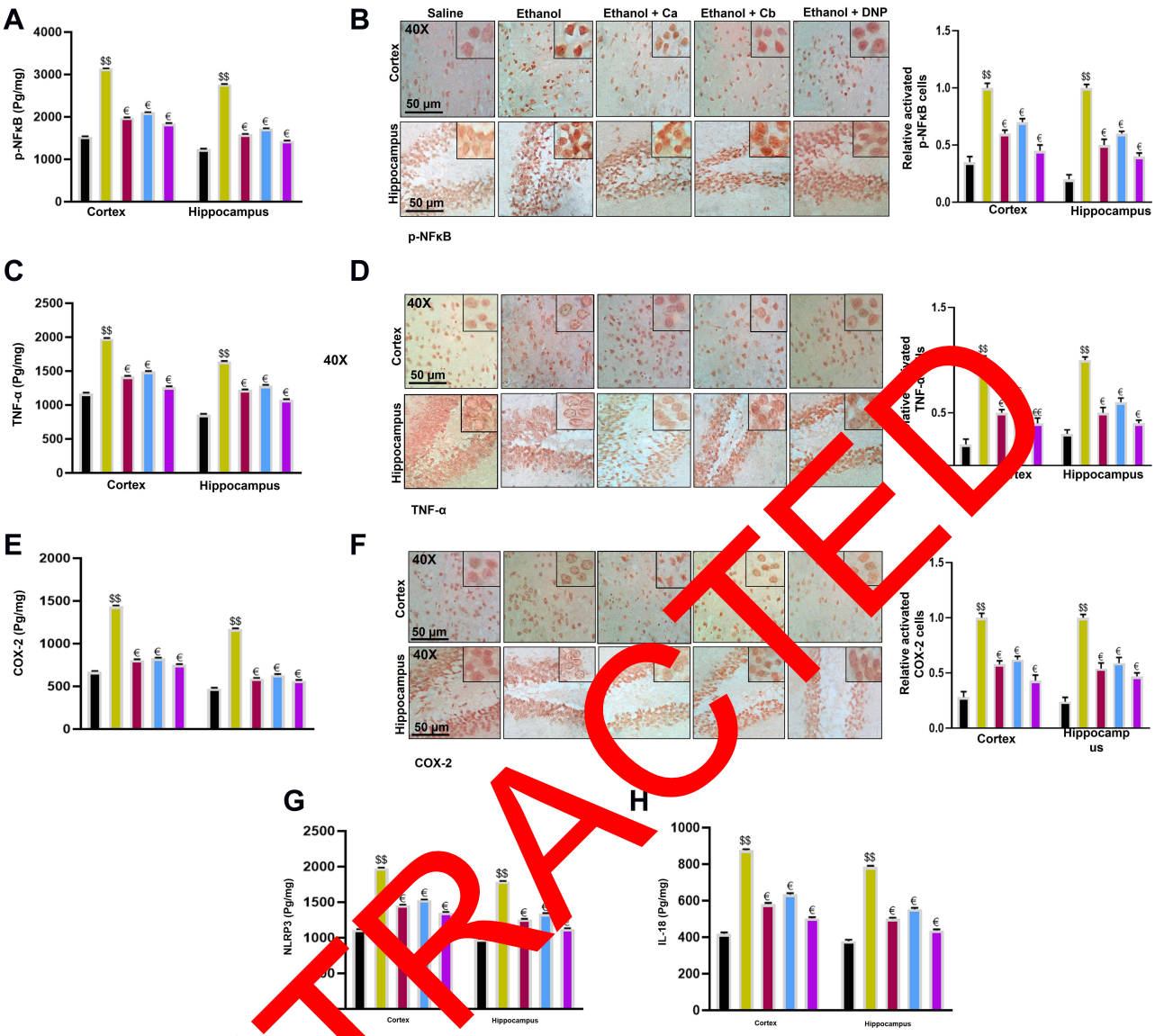

Figure 10 Effect of test compounds on the outcomes of ethanol-induced inflammatory mediators. (**A**) p-NFκB protein expression as quantified by ELISA with (n=5/group). (**B**) Immunohistochemistry results for p-NFκB in the cortical and hippocampal tissues with (n=5/group). p-NF-KB exhibited nucleus localization in the treated tissue. (**C**) TNF-α protein expression as quantified by ELISA with (n=5/group). (**D**) Immunohistochemistry results for TNF-α in the cortical and hippocampal tissues with (n=5/group). TNF-α exhibited cytoplasmic localization in treated brain tissues. (**E**) COX2 protein expression as quantified by ELISA with (n=5/group). (**F**) Immunohistochemistry results for COX2 in the cortical and hippocampal tissues with (n=5/group). (**G**) NLRP3 protein expression as by ELISA (**H**) IL-18 protein expression as by ELISA with (n=5/group). Data are expressed as mean ± SD. $$p<0.01 compared to the saline group, €Shows a significant difference relative to the ethanol group denotes a significant difference compared with the saline group.

(Figure 11, $$p<0.01). Ca and Cb decreased the expression of IL-1β and Caspase-1, which was significantly low compared to the ethanol-treated group €€p<0.01.

Discussion

The benzimidazole core has been reported in many pharmaceutical formulations in recent years due to its high pharmacological activities.[35] More interestingly, these molecules have a diverse application and are marketed as potential candidate drugs against various disorders and are recently reviewed.[4,36] Keeping in view the pharmacological importance, including its safety records and BBB penetration, we have synthesized a new series of benzimidazole derivatives that can target multiple steps of the inflammatory cascade. For this purpose, a multi-reaction scheme was adopted with

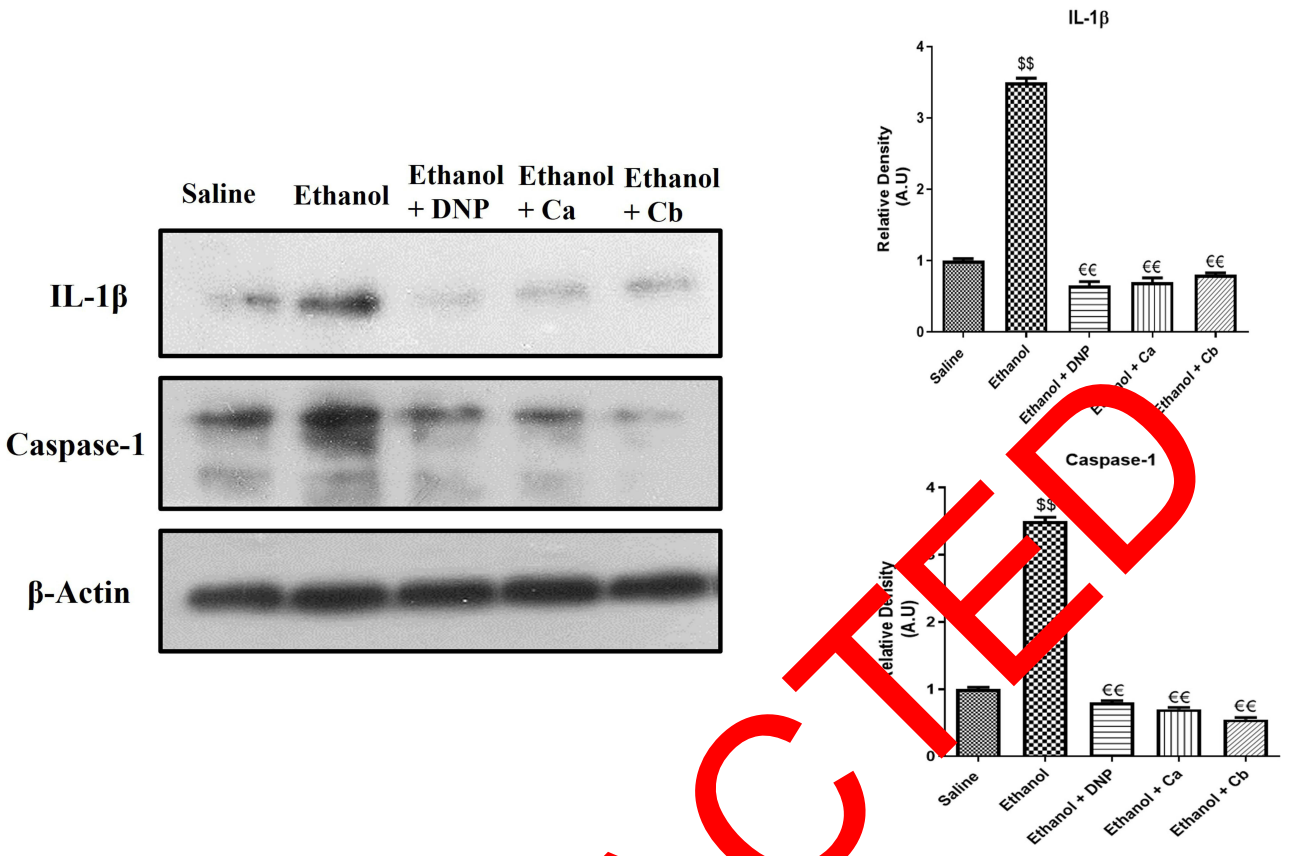

Figure 11 Western blot analysis of IL-1β and Caspase 1. Data are expressed as m[illegible] an [illegible]. $^{\$\$}p<0.01$, $^{**}p<0.01$ compared to the saline group while $^{€€}p<0.05$ compared to the LPS group.

slight modification, as shown in Figure [illegible]. Briefly, the benzimidazole moiety was generated by the reaction of phenylenediamine with different aldehyde[illegible] in the presence of sodium metabisulfite. Then, acetanilide was added to chlorosulfonic acid and stirred at room temperature to generate 4-acetamidobenzene-1-sulfonyl chloride. Finally, the newly synthesized benzimidazole (0.01 mmol) were treated with 4-acetamidobenzene-1-sulfonyl chloride in the presence of sodium hydroxide to produce the final compounds. FTIR, proton NMR (1H-NMR), and carbon-13 (13C-NMR) spectra were used to confirm the resulting derivatives as shown in result section. Most neurodegenerative disorders are characterized by complicated pathophysiology owing to the complex brain nature, and for this reason, several clinical testing. Benzodiazepine moieties can easily permeate the BBB and target several intracellular proteins and ion channels.[37,38]

We previously synthesized different derivatives of benzimidazoles and evaluated their potential anti-inflammatory activities.[15] Those reported compounds exhibited free radical scavenging and antioxidant properties, attenuated neuroinflammation in the memory impairment model. Furthermore, benzimidazole derivatives can target multiple Alzheimer's biomarkers to execute the neuroprotective actions.[16] We previously demonstrated that benzimidazole mediates anti-inflammatory effects by inhibiting inflammatory cytokines,[15] which is consistent with other findings.[17] In this study, we examined whether the newly synthesized derivatives can modulate ethanol-induced memory impairment and cognitive deficits. Furthermore, we demonstrated the neuroprotective effects of benzimidazole against inflammasome (NLRP3). To further support our notion, we performed molecular simulation studies, and both synthetic compounds Ca and Cb exhibited an excellent binding affinity with targets (TNF-α and NLRP3). Ethanol provokes behavioral deficits as several studies ruled out the link of ethanol to dementia and Alzheimer's disease.[39,40] This is because ethanol can lead to irretrievable loss of white matter[41] and sometimes gray matter.[42]

Compound Ca and Cb therapy improved memory in ethanol-treated rats by reducing escape latency during the trial session and boosting the percentage of spontaneous alternation behavior in the Y-maze test.

Furthermore, there is a definite link between increased ROS and inflammatory pathway activation.[43] Many studies have found a link between the activation of inflammatory pathways and the accumulation of oxidative stress with ethanol consumption.[39,44] Elevated oxidative stress affects brain tissues due to the higher oxygen demand and fewer antioxidant enzymes.[40,41] Thus, successful therapeutic approaches should control the neuroinflammation and attenuate oxidative stress via stimulating the antioxidant enzymes. Several studies reported benzimidazole derivatives' antioxidant and anti-inflammatory activities.[11,12,45–49] GSH and GST are essential endogenous antioxidants that help to eliminate free radicals. Benzimidazole derivatives are effective ROS inhibitors via activating GSH and inhibiting LPO.[49,50] Pretreatment using selected benzimidazole significantly increased the combat of the brain against ethanol-induced oxidative stress.

Neuroinflammation triggers ROS release, which is responsible for oxidative stress and aids in exacerbating the pathogenesis of neurodegenerative diseases, including memory impairment, cognitive deficits, and other behavioral abnormalities.[51] Activation of the NLRP3 inflammasome has been linked to the development of several diseases and inflammatory disorders, particularly age-related diseases, such as Alzheimer's disease and type II diabetes (T2D).[52,53] The cellular damage and lipid peroxidation are caused by the generation of reactive oxygen species (ROS) and pro-inflammatory mediators such as interleukin-1 (IL-1) and tumor necrosis factor-alpha (TNF-α).[54] Inhibition of TNF-α helps to alleviate not only inflammation but also cognitive deficits.[55] Inflammasomes are a vital component of the innate immune system[56] comprised multiprotein complex assembled in the cytosol for an executable pro-inflammatory response.[57] Among the various types of the inflammasome, the NLRP3 has been extensively studied in neurodegenerative disorders.[58] Several compounds have been screened and in the early stage of development as potential inhibitors of NLRP3 inflammasome activation.[43]

The involvement of oxidative stress and ROS is consistently reiterated in the pathophysiology of various neurological disorders, including ethanol-induced neurodegeneration. Likewise, oxidative stress can exacerbate dementia as the brain has limited antioxidants combating capacity.[50] Moreover, the degree of oxidative damage is proportional to ethanol consumption.[59] Our results attest to the previously reported data that ethanol administration induces an imbalance between endogenous antioxidant substances and stress agents, thereby stimulating ROS production and activating the neuroinflammatory cascade. Furthermore, several clinically used neuroprotective drugs currently have potential ROS ameliorating effects in patients. Activation of pro-inflammatory mediators like COX-2 and p-NFB, as well as other inflammatory cytokines like interleukin-6 (IL-6), interleukin-1 (IL-1b), and TNF-α, have been implicated in neuronal damage in a variety of neurodegenerative scenarios, including ethanol-induced neurodegeneration.[61] COX2 inhibitors could be potential treatment strategies for attenuating neuroinflammation.[62] Similarly, several TNF-α inhibitors are under human clinical trials for neuroprotective effects.[63]

In conclusion, neuroinflammation causes the release of ROS, which is responsible for oxidative stress, and aids in exacerbating the pathogenesis of neurodegenerative diseases (Figure 10). Neuroinflammation also activates different inflammatory cytokines and mediators such as COX2, TNF-α, and NF-κB.[46] The neuroprotective effects of benzimidazole derivatives are promoted by their free radical scavenging activity, augmentation of endogenous antioxidant proteins (GST, GSH), and amelioration of LPO and other pro-inflammatory mediators (Figure 10). Furthermore, there is a direct link between increased ROS and activation of the inflammatory pathway.[31] Compared to the saline group, the ethanol group showed a significant decrease in GSH and GST levels, indicating an increased level of ROS production in the cortex and hippocampus. Our results supported the hypothesis that benzimidazole derivatives can reduce ethanol-induced neuronal toxicity by regulating the expression of cytokines, antioxidant enzymes, and the inflammatory cascade. The present study outlined the protective effects of novel benzimidazole analogs by targeting the NLRP3 inflammasome, which plays a role in neuroinflammation (Figures 11 and 12).

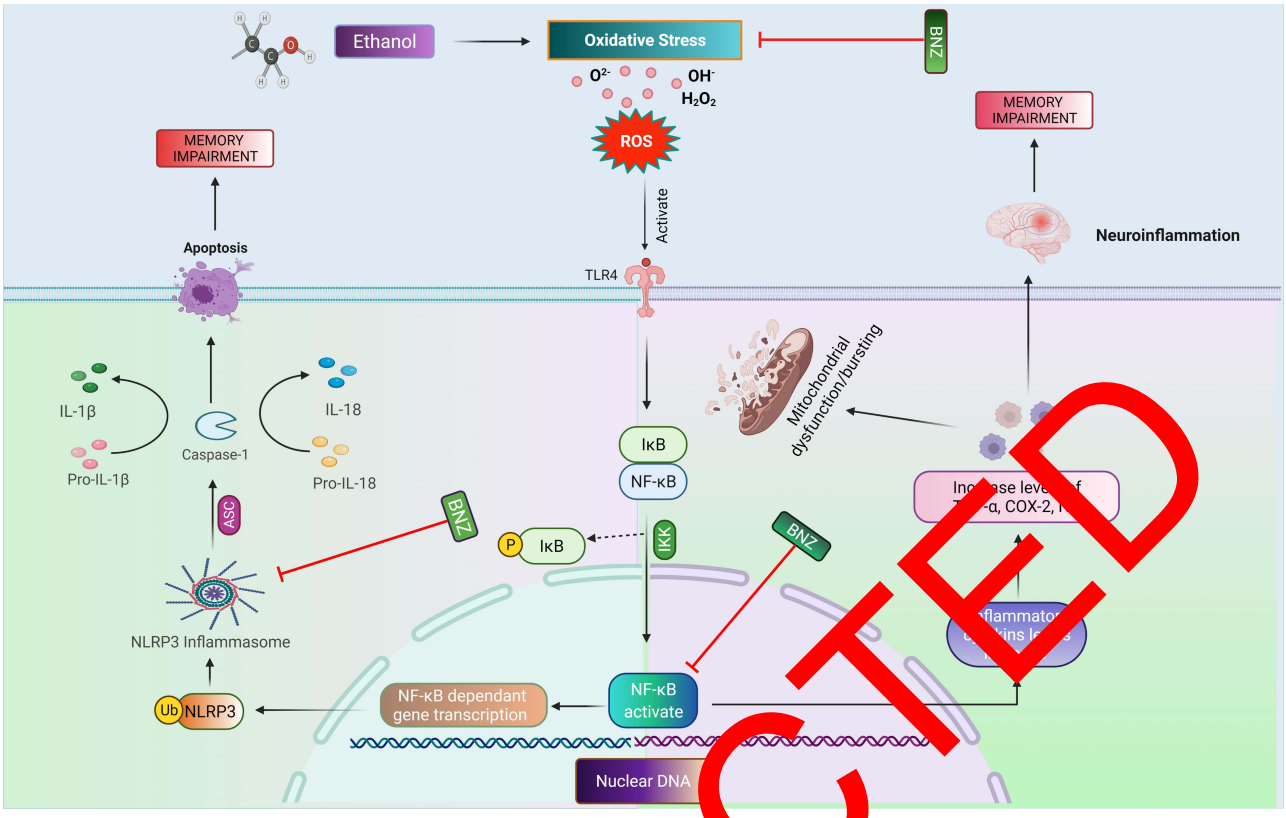

Figure 12 Diagrammatic illustration elaborating the underlying antioxidant and neuroprotective [illegible] of [illegible] and Cb in ethanol-induced memory impairment model.

Institutional Review Board Statement

The protocols were approved by the Research and Ethics Committee (REC) of Riphah International University (REC/RIPS/2021/01).

Acknowledgments

Yusuf S. Althobaiti was supported by Taif University Researchers Supporting Project number (TURSP-2020/78), Taif University, Taif, Saudi Arabia.

Disclosure

The authors declare no conflict of interest in this work.

References

1. Heemels M-T. Neurodegenerative diseases. *Nature*. 2016;539(7628):179–180. doi:10.1038/539179a
2. Jinawath N, Bunbanjerdsuk S, Chayanupatkul M, et al. Bridging the gap between clinicians and systems biologists: from network biology to translational biomedical research. *J Transl Med*. 2016;14(1):1–13. doi:10.1186/s12967-016-1078-3
3. Mott M, Koroshetz W. Bridging the gap in neurotherapeutic discovery and development: the role of the National Institute of Neurological Disorders and Stroke in translational neuroscience. *Neurotherapeutics*. 2015;12(3):651–654. doi:10.1007/s13311-015-0366-6
4. Keri RS, Hiremathad A, Budagumpi S, et al. Comprehensive review in current developments of benzimidazole-based medicinal chemistry. *Chem Biol Drug Des*. 2015;86(1):19–65. doi:10.1111/cbdd.12462
5. El-Feky SA, Abd El-Samii ZK, Osman NA, et al. Synthesis, molecular docking and anti-inflammatory screening of novel quinoline incorporated pyrazole derivatives using the Pfitzinger reaction II. *Bioorg Chem*. 2015;58:104–116. doi:10.1016/j.bioorg.2014.12.003
6. Evans CW, Atkins C, Pathak A, et al. Benzimidazole analogs inhibit respiratory syncytial virus G protein function. *Antiviral Res*. 2015;121:31–38. doi:10.1016/j.antiviral.2015.06.016
7. Hranjec M, Pavlović G, Karminski-Zamola G. Synthesis, crystal structure determination and antiproliferative activity of novel 2-amino-4-aryl-4, 10-dihydro [1, 3, 5] triazino [1, 2-a] benzimidazoles. *J Mol Struct*. 2012;1007:242–251. doi:10.1016/j.molstruc.2011.10.054

8. Anastassova N, Yancheva D, Hristova-Avakumova N, et al. New benzimidazole-aldehyde hybrids as neuroprotectors with hypochlorite and superoxide radical-scavenging activity. *Pharmacol Rep*. 2020;72(4):846–856. doi:10.1007/s43440-020-00077-3
9. Anastassova N, Argirova M, Yancheva D, et al. In vitro assessment of the neuroprotective and antioxidant properties of new benzimidazole derivatives as potential drug candidates for the treatment of Parkinson's disease. *Multidisciplin Digit Publ Instit Proc*. 2019;22(1):54.
10. Anastassova N, Aluani D, Kostadinov A, et al. Evaluation of the combined activity of benzimidazole arylhydrazones as new anti-Parkinsonian agents: monoamine oxidase-B inhibition, neuroprotection and oxidative stress modulation. *Neural Regener Res*. 2021;16(11):2299. doi:10.4103/1673-5374.309843
11. Gurjar AS, Solanki VS, Meshram AR, et al. Exploring beta amyloid cleavage enzyme-1 inhibition and neuroprotective role of benzimidazole analogues as anti-Alzheimer agents. *J Chin Chem Soc*. 2020;67(5):864–873. doi:10.1002/jccs.201900200
12. Gao C, Li B, Zhang B, et al. Synthesis and biological evaluation of benzimidazole acridine derivatives as potential DNA-binding and apoptosis-inducing agents. *Bioorg Med Chem*. 2015;23(8):1800–1807. doi:10.1016/j.bmc.2015.02.036
13. Imran M, Al Kury LT, Nadeem H, et al. Benzimidazole containing acetamide derivatives attenuate neuroinflammation and oxidative stress in ethanol-induced neurodegeneration. *Biomolecules*. 2020;10(1):108. doi:10.3390/biom10010108
14. Gulcan HO, Mavideniz A, Sahin MF, et al. Benzimidazole-derived compounds designed for different targets of Alzheimer's disease. *Curr Med Chem*. 2019;26(18):3260–3278. doi:10.2174/0929867326666190124123208
15. Becaria A, Bondy SC, Campbell A. Aluminum and copper interact in the promotion of oxidative but not inflammatory events: implications for Alzheimer's disease. *J Alzheimers Dis*. 2003;5(1):31–38. doi:10.3233/JAD-2003-5105
16. Qiao Y, Wang P, Qi J, et al. TLR-induced NF-κB activation regulates NLRP3 expression in murine macrophages. *FEBS Lett*. 2012;586(7):1022–1026. doi:10.1016/j.febslet.2012.02.045
17. Muñoz-Planillo R, Kuffa P, Martínez-Colón G, et al. K+ efflux is the common trigger of NLRP3 inflammasome activation by bacterial toxins and particulate matter. *Immunity*. 2013;38(6):1142–1153. doi:10.1016/j.immuni.2013.05.016
18. Jiang H, Yan Y, Jiang W, et al. NLRP3 inflammasome: activation, regulation, and role in diseases. *SCIENTIA SINICA Vitae*. 2017;47(1):125. doi:10.1360/N052016-00360
19. Franchi L, Eigenbrod T, Muñoz-Planillo R, et al. The inflammasome: a caspase-1-activation platform that regulates immune responses and disease pathogenesis. *Nat Immunol*. 2009;10(3):241–247. doi:10.1038/ni.1703
20. Gong Z, Pan J, Shen Q, et al. Mitochondrial dysfunction induces NLRP3 inflammasome activation during cerebral ischemia/reperfusion injury. *J Neuroinflammation*. 2018;15(1):242. doi:10.1186/s12974-018-1282-6
21. Toma C, Higa N, Koizumi Y, et al. Pathogenic vibrio activate NLRP3 inflammasome via cytotoxin and TLR/nucleotide-binding oligomerization domain-mediated NF-κB signaling. *J Immunol*. 2010;184(9):5287–5297. doi:10.4049/jimmunol.0903536
22. Alaqeel SI. Synthetic approaches to benzimidazoles from o-phenylenediamine: a literature review. *J Saudi Chem Soc*. 2017;21(2):229–237. doi:10.1016/j.jscs.2016.08.001
23. Keerthi DS. Chlorosulfonation of acetanilide to obtain an intermediate for the preparation of a sulfa drug. *Asian J Pharma*. 2017;11(01). doi:10.22377/ajp.v11i01.1099
24. Hay LA, Koenig TM, Ginah FO, et al. Palladium-catalyzed hydroarylation of propiolamides. A regio-and stereocontrolled method for preparing 3, 3-diarylacrylamides. *J Org Chem*. 1998;63(15):5050–5058. doi:10.1021/jo9[illegible]5h
25. Bowers KJ, Chow DE, Xu H, et al. *Scalable algorithms for molecular dynamics simulations on commodity clusters*. In: *SC'06: Proceedings of the 2006 ACM/IEEE Conference on Supercomputing*. IEEE; 2006.
26. Shah FA, Rashid S, Rashid S. Conformational ensemble of non-peptide ω-conotoxin mimetics and Ca+ 2 ion binding to human voltage-gated N-type calcium channel Cav2. 2. *Comput Struct Biotechnol J*. 2020;18:2357–2372. doi:10.1016/j.csbj.2020.08.027
27. Al Kury LT, Zeb A, Abidin ZU, et al. Neuroprotective effects of melatonin and celecoxib against ethanol-induced neurodegeneration: a computational and pharmacological approach. *Drug Des Devel Ther*. 2019;13:2715. doi:10.2147/DDDT.S207310
28. Iqbal S, Shah FA, Naeem K, et al. Succinamide derivatives ameliorate neuroinflammation and oxidative stress in scopolamine-induced neurodegeneration. *Biomolecules*. 2020;10(3):443. doi:10.3390/biom10030443
29. Khan A, Shal B, Naveed M, et al. Matrine ameliorates anxiety and depression-like behaviour by targeting hyperammonemia-induced neuroinflammation and oxidative stress in CCl4 model of liver injury. *Neurotoxicology*. 2019;72:38–50. doi:10.1016/j.neuro.2019.02.002
30. Kumar KS, Hsieh TW, Wang S-Y. Anti-inflammatory effect of lucidone in mice via inhibition of NF-κB/MAP kinase pathway. *Int Immunopharmacol*. 2010;10(4):385–392. doi:10.1016/j.intimp.2009.12.013
31. Firdous A, Sarwar S, Shah FA, et al. Contribution of attenuation of TNF-α and NF-κB in the anti-epileptic, anti-apoptotic and neuroprotective potential of [illegible] webbianus fruit and its chitosan encapsulation. *Molecules*. 2021;26(8):2347. doi:10.3390/molecules26082347
32. Ullah I, Badshah H, Mahmood Z, et al. Hepatoprotective effects of melatonin and celecoxib against ethanol-induced hepatotoxicity in rats. *Immunopharmacol Immunotoxicol*. 2020;42(3):255–263. doi:10.1080/08923973.2020.1746802
33. Al Kury LT, Yayyat[illegible] Shah F, et al. Ginkgo biloba extract protects against methotrexate-induced hepatotoxicity: a computational and pharmacological approach. *Molecules*. 2020;25(11):2540. doi:10.3390/molecules25112540
34. Shah FA, Zeb A, Ali T, et al. Identification of proteins differentially expressed in the striatum by melatonin in a middle cerebral artery occlusion rat model—a proteomic and in silico approach. *Front Neurosci*. 2018;12:888. doi:10.3389/fnins.2018.00888
35. Akhtar W, Khan MF, Verma G, et al. Therapeutic evolution of benzimidazole derivatives in the last quinquennial period. *Eur J Med Chem*. 2017;126:705–753. doi:10.1016/j.ejmech.2016.12.010
36. Tahlan S, Kumar S, Ramasamy K, et al. Design, synthesis and biological profile of heterocyclic benzimidazole analogues as prospective antimicrobial and antiproliferative agents. *BMC Chem*. 2019;13(1):1–15.
37. Harada R, Okamura N, Furumoto S, et al. Use of a benzimidazole derivative BF-188 in fluorescence multispectral imaging for selective visualization of tau protein fibrils in the Alzheimer's disease brain. *Mol Imaging Biol*. 2014;16(1):19–27. doi:10.1007/s11307-013-0667-2
38. Ortiz-Guerrero G, Amador-Muñoz D, Calderón-Ospina CA, et al. Proton pump inhibitors and dementia: physiopathological mechanisms and clinical consequences. *Neural Plast*. 2018;2018:1–9. doi:10.1155/2018/5257285
39. Brown SA, Tapert SF, Granholm E, et al. Neurocognitive functioning of adolescents: effects of protracted alcohol use. *Alcohol Clin Exp Res*. 2000;24(2):164–171. doi:10.1111/j.1530-0277.2000.tb04586.x
40. Ridley NJ, Draper B, Withall A. Alcohol-related dementia: an update of the evidence. *Alzheimers Res Ther*. 2013;5(1):3. doi:10.1186/alzrt157

41. Pfefferbaum A, Sullivan EV, Mathalon DH, et al. Frontal lobe volume loss observed with magnetic resonance imaging in older chronic alcoholics. *Alcohol Clin Exp Res*. 1997;21(3):521–529. doi:10.1111/j.1530-0277.1997.tb03798.x
42. Harper C. The neuropathology of alcohol-specific brain damage, or does alcohol damage the brain? *J Neuropathol Exp Neurol*. 1998;57 (2):101–110. doi:10.1097/00005072-199802000-00001
43. White CS, Lawrence CB, Brough D, et al. Inflammasomes as therapeutic targets for A lzheimer's disease. *Brain Pathol*. 2017;27(2):223–234. doi:10.1111/bpa.12478
44. Carugo O. How root-mean-square distance (rmsd) values depend on the resolution of protein structures that are compared. *J Appl Crystallogr*. 2003;36(1):125–128. doi:10.1107/S0021889802020502
45. Qin L, Crews FT. NADPH oxidase and reactive oxygen species contribute to alcohol-induced microglial activation and neurodegeneration. *J Neuroinflammation*. 2012;9(1):1–19. doi:10.1186/1742-2094-9-5
46. Yin J, Valin KL, Dixon ML, Leavenworth JW. The role of microglia and macrophages in CNS homeostasis, autoimmunity, and cancer. *J Immunol Res*. 2017;2017:5150678.
47. Rao J, Rapoport S, Kim H. Altered neuroinflammatory, arachidonic acid cascade and synaptic markers in postmortem Alzheimer's disease brain. *Transl Psychiatry*. 2011;1(8):e31–e31. doi:10.1038/tp.2011.27
48. Dean B, Tawadros N, Scarr E, et al. Regionally-specific changes in levels of tumour necrosis factor in the dorsolateral pr[illegible]ntal cortex obtained postmortem from subjects with major depressive disorder. *J Affect Disord*. 2010;120(1–3):245–248. doi:10.1016/j.jad[illegible]009.04.0[illegible]
49. Maes M, Stevens WJ, Declerck LS, et al. Significantly increased expression of T-cell activation markers (interleukin[illegible] and HLA-DR[illegible] depression: further evidence for an inflammatory process during that illness. *Prog Neuropsychopharmacol Biol Psychiatry*. 199[illegible]17(2):241–255[illegible]oi:10.1016/0278-5846(93)90045-T
50. Freitas R. Investigation of oxidative stress involvement in hippocampus in epilepsy model induced b[illegible] pilocarpine. *N[illegible]rosci[illegible]ett*. 2009;462 (3):225–229. doi:10.1016/j.neulet.2009.07.037
51. Pascual M, Blanco AM, Cauli O, et al. Intermittent ethanol exposure induces inflammatory brain d[illegible]mage[illegible]d causes long-term behavioural alterations in adolescent rats. *Eur J Neurosci*. 2007;25(2):541–550. doi:10.1111/j.1460-9568.200[illegible]05298[illegible]
52. Halle A, Hornung V, Petzold GC, et al. The NALP3 inflammasome is involved in the innate i[illegible]mune respon[illegible]to amy[illegible]d-β. *Nat Immunol*. 2008;9 (8):857–865. doi:10.1038/ni.1636
53. Lee H-M, Kim -J-J, Kim HJ, et al. Upregulated NLRP3 inflammasome activation in pat[illegible]nts wit[illegible]pe 2 diabetes. *Diabetes*. 2013;62(1):194–204. doi:10.2337/db12-0420
54. Mittal M, Siddiqui MR, Tran K, et al. Reactive oxygen species in inflammation[illegible]d tissue injury. *Antio[illegible]d Redox Signal*. 2014;20(7):1126–1167. doi:10.1089/ars.2012.5149
55. Bortolato B, Carvalho A, Soczynska J, et al. The involvement of TNF-α in [illegible]gnitive dysfun[illegible]on associated with major depressive disorder: an opportunity for domain specific treatments. *Curr Neuropharmacol*. 2015;13(5[illegible]58–576. doi:1[illegible]2174/1570159X13666150630171433
56. Ting JP-Y, Lovering RC, Alnemri ES, et al. The NLR gene family: a stand[illegible]d nomencla[illegible]re. *Immunity*. 2008;28(3):285–287. doi:10.1016/j.immuni.2008.02.005
57. Martinon F, Burns K, Tschopp J. The inflammasome: a molecular p[illegible]tform[illegible]ering activation of inflammatory caspases and processing of proIL-β. *Mol Cell*. 2002;10(2):417–426. doi:10.1016/S1097-2765(02)0059[illegible]3
58. Fann DY-W, Lee S-Y, Manzanero S, et al. Intravenous im[illegible]noglobul[illegible]ppresses NLRP1 and NLRP3 inflammasome-mediated neuronal death in ischemic stroke. *Cell Death Dis*. 2013;4(9):e790–e79[illegible]doi:[illegible]1038/cd[illegible].2013.326
59. Hernández JA, López-Sánchez RC, Rendón-Ram[illegible]z A. Lip[illegible]s and ox[illegible]tive stress associated with ethanol-induced neurological damage. *Oxid Med Cell Longev*. 2016;2016:1–15. doi:10.1155/[illegible]16/1543[illegible]
60. Tanner CM. Is the cause of Parkinson's dis[illegible]e env[illegible]p[illegible]ental or hereditary? Evidence from twin studies. *Adv Neurol*. 2003;91:133–142.
61. DeLegge M, Smoke A. Neurodegenerati[illegible]and Inflam[illegible]tion. *Nutr Clin Pract*. 2008;23:35–41. doi:10.1177/011542650802300135
62. Dembo G, Park SB, Kharasch ED. C[illegible]nervous syste[illegible]concentrations of cyclooxygenase-2 inhibitors in humans. *Anesthesiology*. 2005;102 (2):409–415. doi:10.1097/00000542-200502[illegible]9-00026
63. McCoy MK, Tansey MG. TN[illegible]signaling in[illegible]ition in the CNS: implications for normal brain function and neurodegenerative disease. *J Neuroinflammation*. 2008;5[illegible]:1–13. doi:10.1186/[illegible]742-2094-5-45